

Journal Pre-proof

Determination of the elastic parameters of a material from a standardized dynamic stiffness testing

Enrique Segovia, Jennifer Torres, Jesús Carbajo, Jaime Ramis, Jorge P. Arenas



PII: S0022-460X(19)30447-X

DOI: <https://doi.org/10.1016/j.jsv.2019.114885>

Reference: YJSVI 114885

To appear in: *Journal of Sound and Vibration*

Received Date: 12 November 2018

Revised Date: 10 June 2019

Accepted Date: 5 August 2019

Please cite this article as: E. Segovia, J. Torres, Jesús. Carbajo, J. Ramis, J.P. Arenas, Determination of the elastic parameters of a material from a standardized dynamic stiffness testing, *Journal of Sound and Vibration* (2019), doi: <https://doi.org/10.1016/j.jsv.2019.114885>.

This is a PDF file of an article that has undergone enhancements after acceptance, such as the addition of a cover page and metadata, and formatting for readability, but it is not yet the definitive version of record. This version will undergo additional copyediting, typesetting and review before it is published in its final form, but we are providing this version to give early visibility of the article. Please note that, during the production process, errors may be discovered which could affect the content, and all legal disclaimers that apply to the journal pertain.

© 2019 Published by Elsevier Ltd.

Determination of the elastic parameters of a material from a standardized dynamic stiffness testing

Enrique Segovia^a, Jennifer Torres^a, Jesús Carbajo^a, Jaime Ramis^a, Jorge P. Arenas^{b,*}

^a*Department of Physics, Systems Engineering and Signal Theory,
Univ. of Alicante, Mail Box 99; 03080 Alicante, Spain*

^b*Institute of Acoustics, Univ. Austral of Chile, PO Box 567, Valdivia, Chile*

Abstract

Viscoelastic layers under floating floors are often used to reduce impact sound. A standardized dynamic stiffness test is routinely used to estimate the performance of a layer as an impact sound isolator. During the test, a material sample is placed between a load plate and a motionless rigid foundation. In this work, equations that provide a useful analytical description of the standardized test are derived. The new analytical approach is linked with the analysis of multilayer elastomeric bearings. The new approach leads to simpler analytical solutions as compared with those of previous studies, which makes them easy to translate into computer codes. The obtained expressions are almost independent of the shape of the boundary and are only dependent on static values such as the area and moments of inertia of the contour. Taking advantage of the new closed-form solutions, it is shown that, under certain restrictions, the analytical approach may be used to experimentally estimate the elastic parameters of a flexible material using a harmonic (frequency-dependent) analysis. It is reported that results obtained using

*Corresponding author, Tel.: +56-63-2221012; fax: +56-63-2221013
Email address: jparenas@uach.cl (Jorge P. Arenas)

the proposed approach are in good agreement with those obtained using a commercial finite element software.

Keywords: dynamic stiffness, elastic layer, elastic parameters, elastomeric bearings

1. Introduction

Although the main objective of this paper is to propose a novel method to determine the elastic parameters of a material based on the results of a standardized dynamic stiffness test, the proposed analytical approach is framed within the analysis of multilayer rubber bearings, which are widely used in civil, mechanical, and automotive engineering applications.

In 1954, Freyssinet [1] proposed the idea of reinforcing rubber blocks with thin steel plates. These rubber bearings combine the vertical stiffness of a rubber pad and the horizontal flexibility of rubber reinforced by thin steel plates perpendicular to the vertical load. Elastomeric bearings are commonly employed to isolate the vibration of machinery, buildings, and bridges. Evaluation of the horizontal, vertical, and bending stiffnesses is very important to predict the dynamic response and to design efficient applications of multilayer elastomeric bearings. Research on the proper design of these vibration-isolation systems for buildings, bridges, nuclear facilities, and other kind of structures has also been reported more recently. They have included theoretical, numerical and experimental studies [2, 3, 4].

To evaluate these stiffnesses, a number of theoretical analyses have been reported in the technical literature, although they used different approaches and assumptions [5]. Among them are the works of Gent and Lindley [6] and Gent and Meinecke [7], in which they assumed use of an incompressible material, and

the studies by Chalhoub and Kelly [8, 9, 10], in which the material was treated as compressible. Although these approaches have presented rigorous solutions to the vibration problem, they have limitations [11]. In all of these works, two types of assumptions were made: kinematic assumptions about deformation and assumptions about the state of stress, which led to the approximate fulfillment of the internal equilibrium equations and rigorous fulfillment of the equilibrium equations at the boundary. These kinds of solutions depend on the shape of the boundary and present some mathematical complexity. Using a different approach, simplified formulae have also been presented to facilitate the design of elastomeric bearings [12].

It has been common to assume that rubber layers are bonded to rigid or flexible supports, that is, no slip at the contact surface on the top and bottom of the layer. The influence of an unbonded condition at interfaces has recently been studied by Konstantinidis and Moghadam [13] by including partial slip at the contact surface, which requires describing the interface using a friction model. They used a simple Coulomb friction model in a strip and circular unbonded layer and observed that even for pads with a high friction coefficient, a part of the pad close to the edge experiences slip. However, the effect of slip is not that critical for unbonded rubber layers with typical bulk-modulus-to-shear-modulus ratio values and large values of a shape factor and friction coefficient [13]. Research on multilayer bearings continues, including theoretical and applied studies [14, 15, 16].

In the present work, a new analytical approach strictly based on the fulfillment of the equations of internal equilibrium will be presented. This approach leads to much simpler analytical expressions that are almost independent of the shape of the boundary, and they depend only on static values such as the area and moments

of inertia of the contour shape.

It should be noted that some previous studies have also considered the rigorous fulfillment of the equations of internal equilibrium, both in statics [17] and in dynamics [4, 18, 19, 20], as well as in their application in the industry [21]. Although these approaches report solutions that also satisfy the equilibrium equations at the boundary, they have been applied only to circular and annular cross-section shapes, as opposed to the greater generality of the solutions presented in this work. In addition, the analytical solutions obtained here are mathematically very simple compared with those of previous studies.

1.1. Dynamic stiffness of an elastic layer

Viscoelastic layers under floating floors are often used to provide sound and vibration reduction [22]. These layers can be treated as simple linear springs that undergo small displacements and can be described by their dynamic stiffness per unit area. A test setup to determine the dynamic stiffness of an elastic material used under a floating floor has been specified in standard ISO 9052-1 (see Fig. 1) [23]. In summary, the test uses a sample of material placed between a steel load plate and a motionless rigid foundation. The mass of a plate of the same dimensions as the sample is 8 kg, which corresponds to a static load of 2 kPa. The plate is excited by an input dynamic force F applied to the center of the load plate. The input force is commonly applied by an instrumented force hammer. The force is measured by a force transducer and the vertical vibration of the load plate is measured by an accelerometer positioned close to the excitation point. The force and acceleration signals are Fourier-transformed to the frequency domain by a dual-channel FFT analyzer. The acceleration frequency response function (acceleration/force) is then obtained.

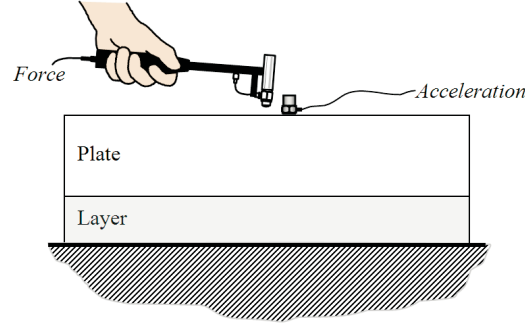


Figure 1: Measurement setup for the determination of the dynamic stiffness of an elastic layer according to the standard ISO 9052-1.

The dynamic stiffness per unit area is defined as the ratio between the applied dynamic force per unit area and the dynamic displacement produced by this force, given by the equation

$$s' = \frac{F/A}{\Delta d}, \quad (1)$$

where A is the surface of the sample, F is the dynamic force acting perpendicular to the sample, and Δd is the resultant dynamic change of thickness of the elastic material.

The ISO standard considers the elastic layer loaded by the plate as analogous to an idealized linear single-degree-of-freedom mass-spring system, and the measurement of the mass-spring resonance frequency is used to calculate the dynamic stiffness according to the standardized test. This resonance frequency, at which the response amplitude is a relative maximum, is

$$f_r = \frac{1}{2\pi} \sqrt{\frac{s'_t}{m'_t}}, \quad (2)$$

where the s'_t and m'_t are the dynamic stiffness per unit area of the sample mate-

rial and the mass per unit area of the load plate used during testing, respectively. Therefore, the apparent dynamic stiffness per unit area is calculated as

$$s'_t = 4\pi^2 m'_t f_r^2. \quad (3)$$

The resonance frequency is determined at a number of different input force levels [24].

During a measurement of dynamic stiffness, if the force and the acceleration are measured at different points on the surface of the plate, a number of close resonance frequencies appear in the frequency response function. An example of the experimental results obtained at five different excitation and response locations in a dynamic stiffness test is shown in Fig. 2. Thus, this fact may be used for obtaining other elastic parameters of the material being tested. The aim of this work is to present a method to estimate the elastic parameters of an elastic layer from experimental results of acceleration. These accelerances are measured using an experimental setup based on standardized dynamic stiffness testing. The elastic layer is viewed as either a non-porous material or a porous material with very high lateral airflow resistivity, ensuring that the effect of the air contained within the material is negligible.

2. Analytical modal analysis

Consider an elastic layer of uniform square cross section A and thickness e , placed between a rigid homogeneous square plate of same cross section A and a rigid motionless foundation. As shown in Fig. 3, a rectangular Cartesian coordinate system is defined relative to an origin located at G^* , where G^* is the mass center of the plate, O is the center point of the lower face of the plate (upper face

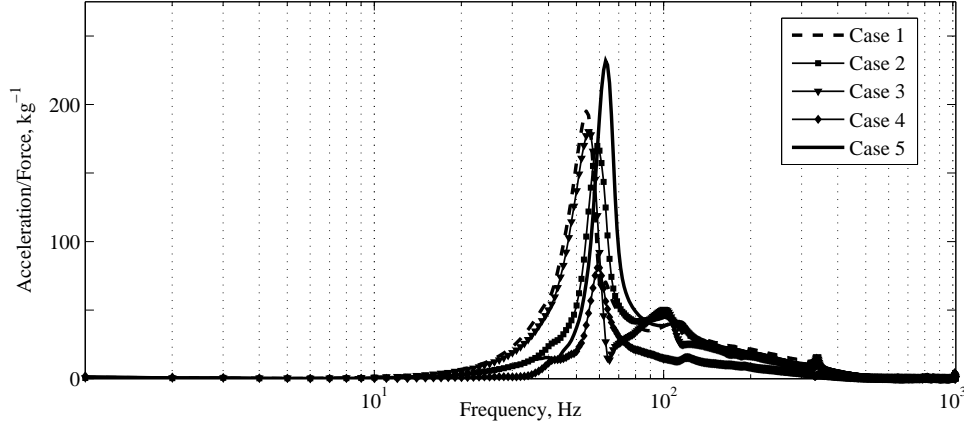


Figure 2: Experimental results of acceleration measured at five different excitation and response locations.

of the elastic layer), and $TXYZ$ is the coordinate system defined relative to an origin T located at the center of the lower face of the elastic layer. Thus $u(x, y, z, t)$, $v(x, y, z, t)$, and $w(x, y, z, t)$ are the displacements of the points of the elastic layer as a function of the coordinates x, y, z and time t . Note that $h = m/\rho_p A$ is the thickness of the plate, where m and ρ_p are the mass and density of the plate, respectively.

The elastic properties of the elastic layer material are described by its Poisson's ratio (ν), Young's modulus (E), bulk modulus (κ), shear modulus (G), Lamé's first parameter (λ), and P-wave modulus (M).

In this work, the following assumptions are made:

1. No slip is allowed at the bonding surface between the plate and the elastic layer or between the elastic layer and the rigid foundation.
2. The plate stiffness is much greater than that of the elastic layer, so the plate

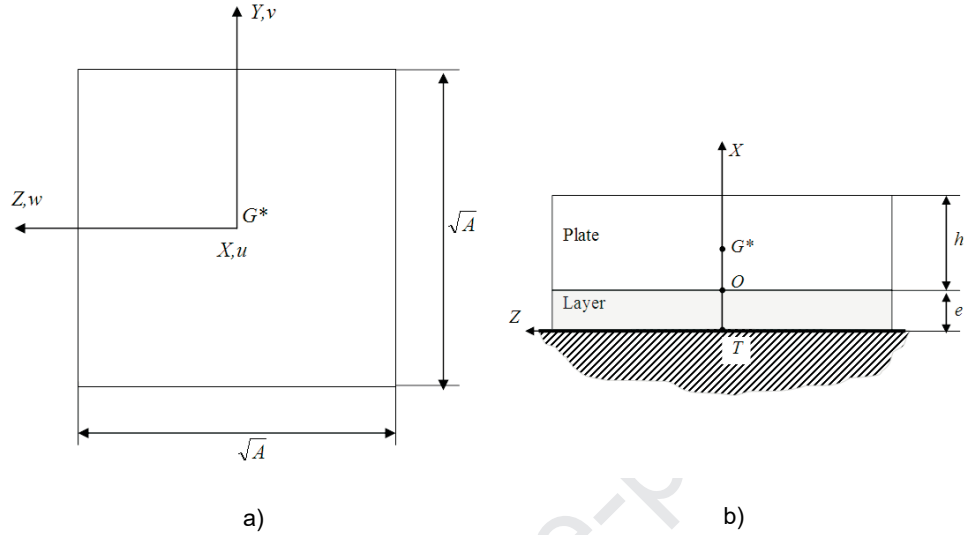


Figure 3: Geometry of the problem: a) top view; b) side view.

can be considered a rigid body.

3. The thickness of the elastic layer is much lesser than its lateral dimension.
4. The displacement gradients in the elastic layer remain sufficiently small throughout the subsequent deformations, so it is permissible to apply the classical linear theory of elasticity.
5. For harmonic analyses, the damping of the plate can be neglected and the damping of the elastic layer can be determined from the imaginary part of their elastic parameters.

A modal analysis is used to find the rigid body modes that can be excited in the plate. Since the plate is assumed to be a rigid body, we can use the fundamental equations for the motion of rigid bodies in three dimensions [25]

$$F_x = m\ddot{u}_{G^*}, \quad (4a)$$

$$F_y = m\ddot{v}_{G^*}, \quad (4b)$$

$$F_z = m\ddot{w}_{G^*}, \quad (4c)$$

$$M_{xG^*} = I_{xG^*}\ddot{\theta}_x, \quad (4d)$$

$$M_{yG^*} = I_{yG^*}\ddot{\theta}_y, \quad (4e)$$

$$M_{zG^*} = I_{zG^*}\ddot{\theta}_z. \quad (4f)$$

where the principal centroidal moments of inertia of the plate are

$$I_{xG^*} = \frac{1}{6}mA, \quad I_{yG^*} = I_{zG^*} = \frac{1}{12}m(A + h^2). \quad (5)$$

To determine the linear and angular displacements of the mass center, we use the following linear approximation [25]

$$\begin{Bmatrix} u \\ v \\ w \end{Bmatrix}_{G^*} \approx \begin{Bmatrix} u \\ v \\ w \end{Bmatrix}_O + \vec{\theta} \times \overrightarrow{OG^*}. \quad (6)$$

Since the plate is a rigid body, the rotations around points O and G^* are identical. Therefore, it is necessary to determine the displacements and rotations around O at the elastic layer. We notice that for the layer $\partial v/\partial y = \partial w/\partial z = 0$ at the interfaces $x = 0$ (foundation) and $x = e$ (plate), and since $\sqrt{A} \gg e$, $\partial v/\partial y = \epsilon_y \approx 0$ and $\partial w/\partial z = \epsilon_z \approx 0$ over most of the elastic layer. Consequently, we can consider that

$$\begin{aligned} u(x, y, z, t) &= u(x, y, z, t), \\ v(x, y, z, t) &\cong v(x, z, t), \\ w(x, y, z, t) &\cong w(x, y, t). \end{aligned} \quad (7)$$

To satisfy the boundary conditions at $x = 0$

$$u(0, y, z, t) = v(0, z, t) = w(0, y, t) = 0. \quad (8)$$

We use the method of separation of variables by writing

$$\begin{aligned} u(x, y, z, t) &= e^{i\omega t} f_u(x) g_u(y, z), \\ v(x, z, t) &= e^{i\omega t} f_v(x) g_v(z), \\ w(x, y, z) &= e^{i\omega t} f_w(x) g_w(y). \end{aligned} \quad (9)$$

Now, the Lamé-Navier equations in Cartesian coordinates are [26]

$$\begin{aligned} \rho \frac{\partial^2 u}{\partial t^2} &= (\lambda + G) \frac{\partial}{\partial x} \left(\frac{\partial u}{\partial x} + \frac{\partial v}{\partial y} + \frac{\partial w}{\partial z} \right) + G \left(\frac{\partial^2 u}{\partial x^2} + \frac{\partial^2 v}{\partial y^2} + \frac{\partial^2 w}{\partial z^2} \right), \\ \rho \frac{\partial^2 v}{\partial t^2} &= (\lambda + G) \frac{\partial}{\partial y} \left(\frac{\partial u}{\partial x} + \frac{\partial v}{\partial y} + \frac{\partial w}{\partial z} \right) + G \left(\frac{\partial^2 u}{\partial x^2} + \frac{\partial^2 v}{\partial y^2} + \frac{\partial^2 w}{\partial z^2} \right), \\ \rho \frac{\partial^2 w}{\partial t^2} &= (\lambda + G) \frac{\partial}{\partial z} \left(\frac{\partial u}{\partial x} + \frac{\partial v}{\partial y} + \frac{\partial w}{\partial z} \right) + G \left(\frac{\partial^2 u}{\partial x^2} + \frac{\partial^2 v}{\partial y^2} + \frac{\partial^2 w}{\partial z^2} \right). \end{aligned} \quad (10)$$

Substitution of Eqs. (9) into (10) yields

$$\begin{aligned} u(x, y, z, t) &= e^{i\omega t} \sin(k_p x) (C_1 y + C_2 z + C_3 + C_8 y z), \\ v(x, z, t) &= e^{i\omega t} \left\{ (C_6 z + C_4) \sin(k_s x) + \frac{C_8 z + C_1}{k_p} (\cos(k_s x) - \cos(k_p x)) \right\}, \\ w(x, y, t) &= e^{i\omega t} \left\{ (C_7 y + C_5) \sin(k_s x) + \frac{C_8 y + C_2}{k_p} (\cos(k_s x) - \cos(k_p x)) \right\}, \end{aligned} \quad (11)$$

where $\alpha = \sqrt{M/\rho}$ is the P-wave velocity, $\beta = \sqrt{G/\rho}$ is the S-wave velocity, $k_p = \omega/\alpha$ is the P-wavenumber, $k_s = \omega/\beta$ is the S-wavenumber, and C_i are arbitrary constants.

To determine the motion of the plate, we must take into account the continuity equations for the interface between the elastic layer and the plate, given by

$$\begin{aligned} u(e, y, z, t) \Big|_{\text{elastic layer}} &= u(e, y, z, t) \Big|_{\text{plate}}, \\ v(e, z, t) \Big|_{\text{elastic layer}} &= v(e, z, t) \Big|_{\text{plate}}, \\ w(e, y, t) \Big|_{\text{elastic layer}} &= w(e, y, t) \Big|_{\text{plate}}. \end{aligned} \quad (12)$$

Therefore, at $x = e$

$$\begin{aligned} \left. \frac{\partial u}{\partial y} \right|_{\text{elastic layer}} &= \left. \frac{\partial u}{\partial y} \right|_{\text{plate}} & ; & \quad \left. \frac{\partial v}{\partial z} \right|_{\text{elastic layer}} = \left. \frac{\partial v}{\partial z} \right|_{\text{plate}} & ; \\ \left. \frac{\partial u}{\partial z} \right|_{\text{elastic layer}} &= \left. \frac{\partial u}{\partial z} \right|_{\text{plate}} & ; & \quad \left. \frac{\partial w}{\partial y} \right|_{\text{elastic layer}} = \left. \frac{\partial w}{\partial y} \right|_{\text{plate}} . \end{aligned} \quad (13)$$

Since the plate is assumed to be elastic deformable, but whose stiffness tends to infinity, the components θ_x , θ_y (see Fig. 4a) and θ_z (see Fig. 4b) for small rotations are

$$\begin{aligned} \theta_x \Big|_{\text{plate}} &= \frac{1}{2} \left(\frac{\partial w}{\partial y} - \frac{\partial v}{\partial z} \right) \Big|_{\text{plate(at } x=e)} = \frac{1}{2} \left(\frac{\partial w}{\partial y} - \frac{\partial v}{\partial z} \right) \Big|_{\text{elastic layer(at } x=e)} , \\ \theta_y \Big|_{\text{plate}} &\approx - \frac{\partial w}{\partial x} \Big|_{\text{plate}} \approx \frac{\partial u}{\partial z} \Big|_{\text{plate}} = \frac{\partial u}{\partial z} \Big|_{\text{elastic layer (at } x=e)} , \\ \theta_z \Big|_{\text{plate}} &\approx \frac{\partial v}{\partial x} \Big|_{\text{plate}} \approx - \frac{\partial u}{\partial y} \Big|_{\text{plate}} = - \frac{\partial u}{\partial y} \Big|_{\text{elastic layer (at } x=e)} . \end{aligned} \quad (14)$$

Note that since the plate' stiffness tends to infinity, the plate shear strain is much greater than that of the elastic layer, so the tensorial shear strain components $\frac{1}{2}\gamma_{xz}$ and $\frac{1}{2}\gamma_{xy}$ of the infinitesimal strain tensor can be neglected in the equations for θ_y and θ_z given by Eq. (14).

The components of the motion of the mass center G^* and those of the plate rotation are calculated through the substitution of u , v , and w from Eq. (11) into

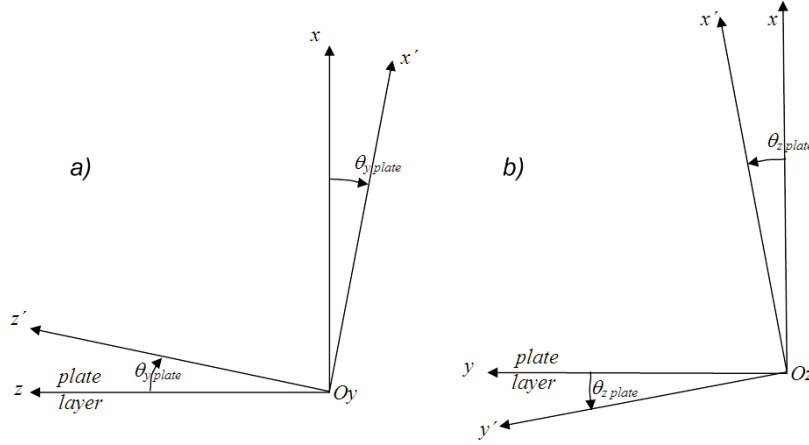


Figure 4: Rotations: a) of the upper face of the layer about Oy ; b) of the upper face of the layer about Oz .

Eqs. (6) and (14). Thus, it follows that

$$\begin{aligned}
 u_{G^*}(t) &= u_0 = e^{i\omega t} C_3 \sin(k_p e), \\
 v_{G^*}(t) &= v_0 + \frac{h}{2} \theta_z \\
 &= e^{i\omega t} \left\{ C_4 \sin(k_s e) + \frac{C_1}{k_p} (\cos(k_s e) - \cos(k_p e)) - \frac{1}{2} C_1 h \sin(k_p e) \right\}, \\
 w_{G^*}(t) &= w_0 - \frac{h}{2} \theta_y \\
 &= e^{i\omega t} \left\{ C_5 \sin(k_s e) + \frac{C_2}{k_p} (\cos(k_s e) - \cos(k_p e)) - \frac{1}{2} C_2 h \sin(k_p e) \right\}, \\
 \theta_x(t) &= e^{i\omega t} \frac{1}{2} (C_7 - C_6) \sin(k_s e), \\
 \theta_y(t) &= e^{i\omega t} (C_8 y + C_2) \sin(k_p e), \\
 \theta_z(t) &= -e^{i\omega t} (C_8 z + C_1) \sin(k_p e).
 \end{aligned} \tag{15}$$

Since the plate is a rigid body, $\theta_x(t)$ and $\theta_z(t)$ do not make sense if $C_8 \neq 0$. In addition, since the layer is bonded to the plate at $x = e$, this surface should move as a rigid plane, i.e., the motion of any point P of coordinates (e, y, z) at that surface, must verify that

$$\begin{pmatrix} u \\ v \\ w \end{pmatrix}_P = \begin{pmatrix} u \\ v \\ w \end{pmatrix}_O + \vec{\theta} \times \vec{OP}, \quad (16)$$

where O is a point with coordinates $(e, 0, 0)$, $\vec{OP} = y\hat{j} + z\hat{k}$, and

$$\vec{\theta} \times \vec{OP} = \begin{vmatrix} \hat{i} & \hat{j} & \hat{k} \\ \theta_x & \theta_y & \theta_z \\ 0 & y & z \end{vmatrix} = (z\theta_y - y\theta_z)\hat{i} - z\theta_x\hat{j} + y\theta_x\hat{k}. \quad (17)$$

To satisfy Eq. (16) we need $C_7 = -C_6$. Therefore, Eqs. (11) and (15) are now

$$\begin{aligned} u(x, y, z, t) &= e^{i\omega t} \sin(k_p x)(C_1 y + C_2 z + C_3), \\ v(x, z, t) &= e^{i\omega t} \left\{ (C_6 z + C_4) \sin(k_s x) + \frac{C_1}{k_p} (\cos(k_s x) - \cos(k_p x)) \right\}, \\ w(x, y, t) &= e^{i\omega t} \left\{ (-C_6 y + C_5) \sin(k_s x) + \frac{C_2}{k_p} (\cos(k_s x) - \cos(k_p x)) \right\}, \end{aligned} \quad (18)$$

and

$$\begin{aligned}
u_{G^*}(t) &= u_0 = e^{i\omega t} C_3 \sin(k_p e), \\
v_{G^*}(t) &= v_0 + \frac{h}{2} \theta_z \\
&= e^{i\omega t} \left\{ C_4 \sin(k_s e) + \frac{C_1}{k_p} (\cos(k_s e) - \cos(k_p e)) - \frac{1}{2} C_1 h \sin(k_p e) \right\}, \\
w_{G^*}(t) &= w_0 - \frac{h}{2} \theta_y \\
&= e^{i\omega t} \left\{ C_5 \sin(k_s e) + \frac{C_2}{k_p} (\cos(k_s e) - \cos(k_p e)) - \frac{1}{2} C_2 h \sin(k_p e) \right\}, \\
\theta_x(t) &= -e^{i\omega t} C_6 \sin(k_s e), \\
\theta_y(t) &= e^{i\omega t} C_2 \sin(k_p e), \\
\theta_z(t) &= -e^{i\omega t} C_1 \sin(k_p e).
\end{aligned} \tag{19}$$

Thus, we need to determine just six unknowns C_i . In order to do this, we express Eq. (4) in terms of the six unknowns C_i , using that

$$\begin{aligned}
(F_x, F_y, F_z) &= \iint (-\sigma_x, -\tau_{xy}, -\tau_{xz}) \Big|_{x=e} dA, \\
(M_{xG^*}, M_{yG^*}, M_{zG^*}) &= \iint (z\tau_{xy} - y\tau_{xz}, -\frac{h}{2}\tau_{xz} - z\sigma_x, \frac{h}{2}\tau_{xy} + y\sigma_x) \Big|_{x=e} dA,
\end{aligned} \tag{20}$$

where σ_x , τ_{xy} , and τ_{xz} are the layer's components of stress at the interface between the layer and the plate ($x = e$). Considering the stress-strain relations [26], the relationship between strains and plate's motion [26], and using u , v and w given by Eq. (18), the unknowns are obtained after integrating the six equations in Eq. (20).

The components of the force and momentum are determined from Eq. (4). From Eq. (4a), $F_x = m\ddot{u}_{G^*}$, we obtain the vibration mode corresponding to pure translation along the x -axis. The natural frequency ω is then determined by solving the transcendental equation $\tan(k_p e) = \tan(e\omega/\alpha) = A\sqrt{M\rho}/m\omega$. When we

perform a standardized experimental determination of the dynamic stiffness of an elastic layer, e and ρ are usually very small quantities such that $k_p e = e\omega/\alpha \ll 1$. So,

$$\tan(k_p e) \approx k_p e = e\omega \sqrt{\frac{\rho}{M}} = \frac{A \sqrt{M\rho}}{m\omega}.$$

Solving for ω in the expression above gives $\omega^2 = MA/em$ and the resonance frequency in Hz is

$$f = \frac{1}{2\pi} \sqrt{\frac{AM}{em}}. \quad (21)$$

Now, by comparing Eqs. (2) and (21) we find that the apparent dynamic stiffness $s'_i = M/e$. Therefore, M can be determined from a measured value of s'_i . This approach is valid when the undamped natural frequency of the system is close to that obtained experimentally.

To determine the other modes of vibration, we substitute Eq. (19) into $F_y = m\ddot{v}_{G^*}$ and $M_{zG^*} = I_{zG^*}\ddot{\theta}_z$ (see Eq. (4)). Manipulation of the equations yields the frequency equation

$$\frac{\omega^2}{12} \{6Ahm \sqrt{GM} \cos^2(k_s e) + 2\mathcal{P}m \sin(k_s e) + A\mathcal{Q} \cos(k_s e)\} = 0, \quad (22)$$

where

$$\mathcal{P} = \frac{-A^2\omega \sqrt{M\rho}}{2} \cos(k_p e) + 3Ah \sqrt{GM} \sin(k_s e) + \left(\frac{\omega^2 m}{2} (A + h^2) - 6AGh \right) \sin(k_p e),$$

and

$$\mathcal{Q} = \sqrt{GM}(A^2\rho - 6hm) \cos(k_p e) - \omega m \sqrt{G\rho}(A + 4h^2) \sin(k_p e),$$

which gives the natural frequencies. A solution of $\omega^2 = 0$ gives two natural frequencies of the vibration modes for a rigid body corresponding to pure translation along the y -axis and rotation about the z -axis. Substitution of Eq. (19) into Eqs. (4c) and (4e) leads to other vibration modes, which have the same natural frequencies since the equations are the same because of the symmetry.

2.1. Numerical Example

A numerical experiment was performed to test the theory presented above. A solid plate ($m = 8$ kg, $h = 0.0255$ m, and $A = 0.04$ m²) on top of an elastic layer ($\rho = 20$ kg/m³, $e = 0.003$ m, $M = 143951$ N/m², and $\nu = 0.45$) has been considered. For comparison, the problem was solved using a commercial finite element program (ANSYS©, Academic Research Mechanical, ver. 19.2). The model consisted of 12800 three-dimensional SOLID186 elements (20 nodes per element) and 58097 nodes with a uniform mesh. The theoretical and numerical results are shown in Figs. 5 to 10.

The six modes of vibration corresponding to the six degrees of freedom of the rigid body plate are determined. In addition, two double natural frequencies are obtained due to symmetry. We see that the theoretical results are in good agreement with those from ANSYS. The differences between the theoretical and numerical natural frequencies were less than 3.4% in all cases.

3. Proposed methodology

In this section, a method for estimating the elastic parameters of the material's layer is proposed. The method is based on the theoretical analysis presented above, but now we include the effects of a harmonic force applied to the plate.

Suppose now that a harmonic force of amplitude F_0 , $F(t) = F_0 e^{i\omega t}$ is applied perpendicular to the top surface of the plate at a point, P , of arbitrary coordinates $(e + h, y_F, z_F)$. Then, we calculate the normal acceleration along the x -axis at a point, Q , which is also located on the top surface of the plate at arbitrary coordinates $(e + h, y_Q, z_Q)$. Thus, we are considering the real conditions during the standardized experimental determination of the dynamic stiffness of an elastic

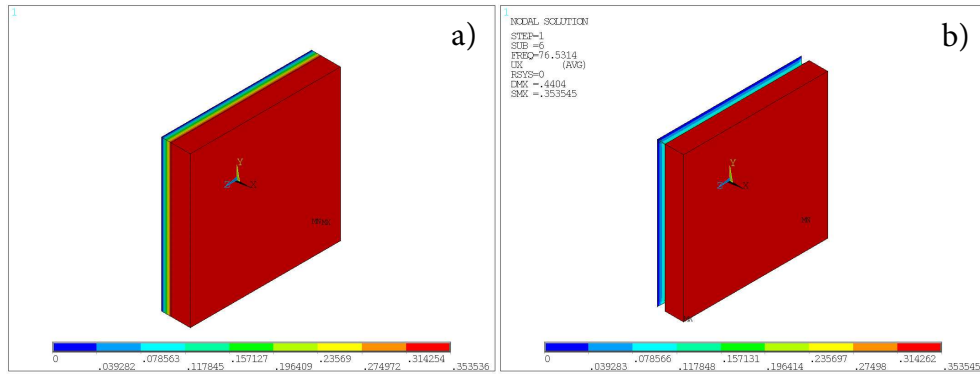


Figure 5: u component of the plate: a) theoretical, Eq. (4a) (77.95 Hz); b) numerical (76.53 Hz).

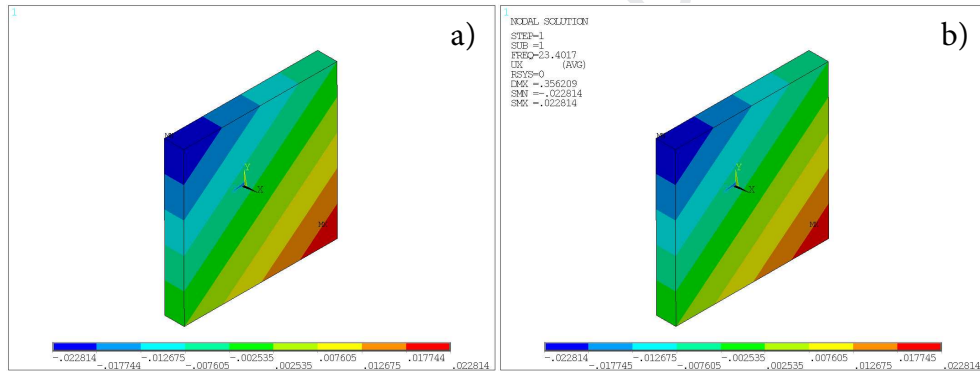


Figure 6: u component of the plate: a) theoretical, Eqs. (4b), (4c), (4e), and (4f) (23.50 Hz double); b) numerical (23.40 Hz double).

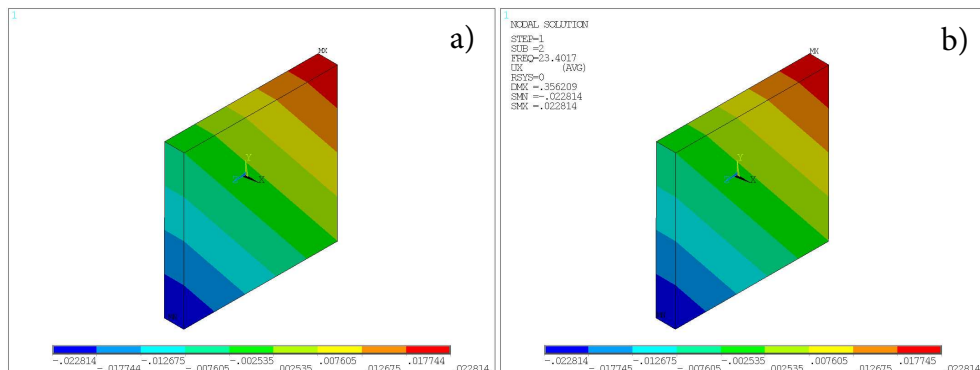


Figure 7: u component of the plate: a) theoretical, Eqs. (4b), (4c), (4e), and (4f) (23.50 Hz double); b) numerical (23.40 Hz double).

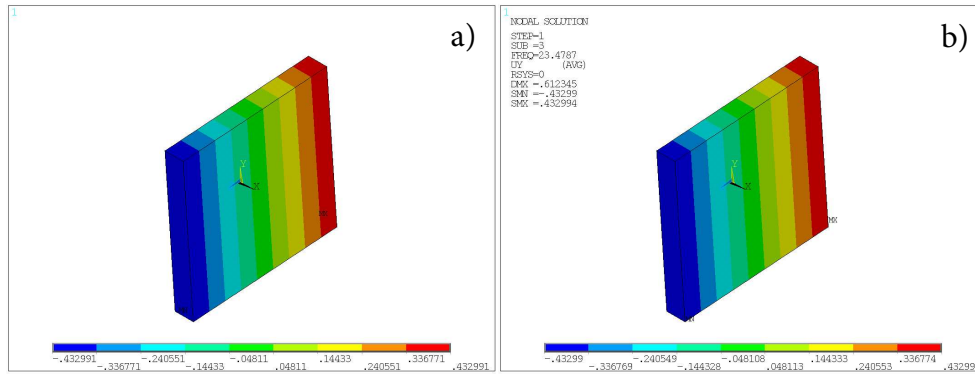


Figure 8: v component of the plate: a) theoretical, Eq. (4d) (23.50 Hz); b) numerical (23.48 Hz).

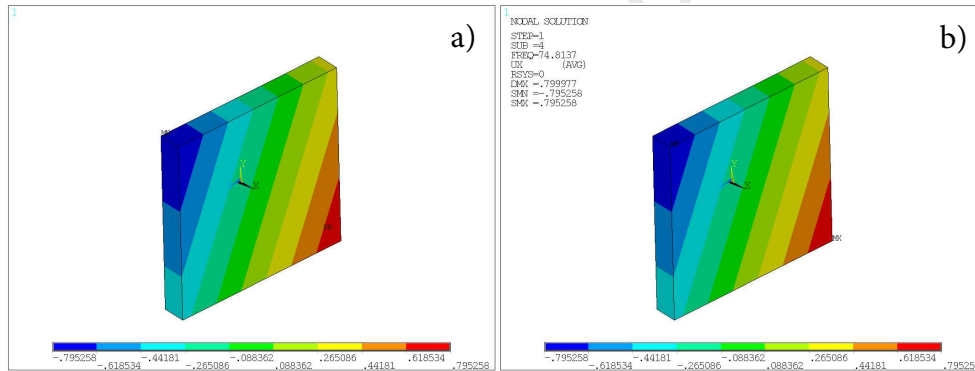


Figure 9: u component of the plate: a) theoretical, Eqs. (4b), (4c), (4e), and (4f) (77.34 Hz double); b) numerical (74.81 Hz double).

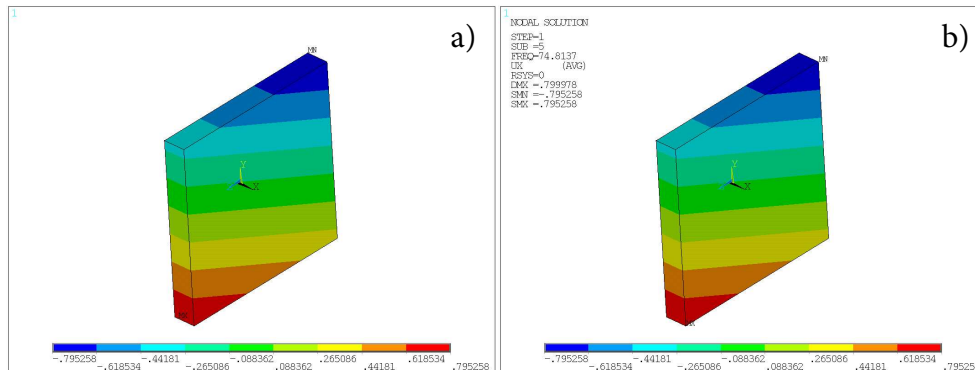


Figure 10: u component of the plate: a) theoretical, Eqs. (4b), (4c), (4e), and (4f) (77.34 Hz double); b) numerical (74.81 Hz double).

material of thickness e .

We must solve the new dynamic equilibrium equations by determining the displacement of the mass center and the rotations of the plate given by Eqs. (4), where we must consider the effects of the applied force, i.e. the resultant force

$$\{F_0 e^{i\omega t}, 0, 0\}, \quad (23)$$

and resultant moment produced by the force about point G^*

$$\overrightarrow{G^*P} \times \{F_0 e^{i\omega t}, 0, 0\} = \begin{vmatrix} \hat{i} & \hat{j} & \hat{k} \\ h/2 & y_F & z_F \\ F_0 e^{i\omega t} & 0 & 0 \end{vmatrix} = F_0 e^{i\omega t} \{0, z_F, -y_F\}. \quad (24)$$

The expressions for the components of the displacement of the mass center G^* and those of the rotation of the plate are given by Eqs. (19), but ω is now the frequency of the excitation force.

Taking the second derivative of Eq. (6) with respect to time, replacing G^* and O with Q and G^* respectively, we obtain the acceleration of point Q as

$$\begin{pmatrix} \ddot{u} \\ \ddot{v} \\ \ddot{w} \end{pmatrix}_Q \approx \begin{pmatrix} \ddot{u} \\ \ddot{v} \\ \ddot{w} \end{pmatrix}_{G^*} + \overrightarrow{\ddot{\theta}} \times \overrightarrow{G^*Q}. \quad (25)$$

Since we just need the acceleration along the x -axis, we have that

$$\ddot{u}_Q = \ddot{u}_{G^*} + \ddot{\theta}_y z_Q - \ddot{\theta}_z y_Q. \quad (26)$$

Calculating the constants C_i that satisfy Eqs. (4), we obtain after some algebra that

$$\ddot{u}_Q = \frac{-\omega^2 F_0 e^{i\omega t}}{A\omega \sqrt{M\rho} \cot(k_p e) - m\omega^2} + F_0 e^{i\omega t} (z_F z_Q + y_F y_Q) f_\theta, \quad (27)$$

where

$$f_\theta = 12\omega \frac{\sin(k_p e)}{\mathcal{R}} \{m\omega \sin(k_s e) - A \sqrt{G\rho} \cos(k_s e)\}, \quad (28)$$

with

$$\mathcal{R} = 6Ahm \sqrt{GM} \cos^2(k_s e) + A\mathcal{Q} \cos(k_s e) + 2m\mathcal{P} \sin(k_s e).$$

Dividing Eq. (27) by $F_0 e^{i\omega t}$, and using the following notation for the acceleration transfer functions

$$\mathcal{A}c_Q = \frac{\ddot{u}_Q}{F_0 e^{i\omega t}}, \quad (29)$$

$$\mathcal{A}c_{G^*} = \frac{\ddot{u}_{G^*}}{F_0 e^{i\omega t}} = \frac{-\omega^2}{A\omega \sqrt{M\rho} \cot(k_p e) - m\omega^2}, \quad (30)$$

yields

$$\mathcal{A}c_Q = \mathcal{A}c_{G^*} + (z_F z_Q + y_F y_Q) f_\theta. \quad (31)$$

Note that the functions in Eq. (31) depend on a set of variables, i.e.,

$$\mathcal{A}c_Q = \mathcal{A}c_Q(\omega, M, \rho, e, A, m, h, G, y_F, z_F, y_Q, z_Q),$$

$$\mathcal{A}c_{G^*} = \mathcal{A}c_{G^*}(\omega, M, \rho, e, A, m), \quad (32)$$

$$f_\theta = f_\theta(\omega, M, \rho, e, A, m, h, G).$$

The Taylor series expansion of function $f_\theta(\omega)$ in Eq. (32) about $\omega = 0$ is given by

$$f_\theta \approx \frac{12e}{A^2 M} \omega^2 + \frac{12Ae^2 m + (108 - 36M/G)e^3 h m + 48e^2 h^2 m + 4A^2 e^3 \rho}{A^4 M^2} \omega^4 + O(\omega^5). \quad (33)$$

Therefore, we notice that if ω is very small,

$$f_\theta \approx \frac{12e\omega^2}{A^2 M} \quad (34)$$

and f_θ does not depend explicitly on the parameter G .

As in the proposed methodology, we will use f_θ in Eq. (32) to find G as a function of frequency ω , which means that the method cannot be used for small frequencies. One way to reduce this limitation is to increase the sensitivity of f_θ when varying G by increasing the factor $(e/A)^2hm$ (see Eq. (33)). However, the accuracy of the solution decreases as we increase e/A , and the plate could become too heavy to handle if we increase m . Therefore, the simplest way to overcome this problem would be to increase h using a material that is lighter and much more rigid than the elastic material.

4. Determination of the elastic parameters of the layer

Let us consider that the values of ρ , e , A , m , and h are known. We need to find the elastic parameters $M(\omega)$ and $G(\omega)$ at each frequency $\omega = 2\pi f$. When performing a standardized dynamic stiffness test, we can obtain two acceleration transfer functions: (a) $\mathcal{A}c_{Q_1}$, which is the acceleration measured at point $Q_1(e + h, y_{Q_1}, z_{Q_1})$ in response to a force applied at point $P_1(e + h, y_{F_1}, z_{F_1})$, and (b) $\mathcal{A}c_{Q_2}$, which is the acceleration measured at point $Q_2(e + h, y_{Q_2}, z_{Q_2})$ in response to a force applied at point $P_2(e + h, y_{F_2}, z_{F_2})$. Therefore, by using Eq. (31) we can write

$$\begin{aligned}\mathcal{A}c_{Q_1} &= \widehat{\mathcal{A}c_{G^*}} + (z_{F_1}z_{Q_1} + y_{F_1}y_{Q_1})\widehat{f}_\theta \\ \mathcal{A}c_{Q_2} &= \widehat{\mathcal{A}c_{G^*}} + (z_{F_2}z_{Q_2} + y_{F_2}y_{Q_2})\widehat{f}_\theta.\end{aligned}\quad (35)$$

The hat symbol indicates that the values are determined experimentally. Equation (35) is a linear system of two equations and two unknowns: $\widehat{\mathcal{A}c_{G^*}}$ and \widehat{f}_θ . The solution for Eq. (35) is

$$\begin{aligned}\widehat{\mathcal{A}c_{G^*}} &= \frac{\mathcal{A}c_{Q_2}y_{F_1}y_{Q_1} - \mathcal{A}c_{Q_1}y_{F_2}y_{Q_2} + \mathcal{A}c_{Q_2}z_{F_1}z_{Q_1} - \mathcal{A}c_{Q_1}z_{F_2}z_{Q_2}}{y_{F_1}y_{Q_1} - y_{F_2}y_{Q_2} + z_{F_1}z_{Q_1} - z_{F_2}z_{Q_2}}, \\ \widehat{f}_\theta &= \frac{\mathcal{A}c_{Q_1} - \mathcal{A}c_{Q_2}}{y_{F_1}y_{Q_1} - y_{F_2}y_{Q_2} + z_{F_1}z_{Q_1} - z_{F_2}z_{Q_2}}.\end{aligned}\quad (36)$$

In Eq. (36), we note that the only condition is that coordinates of points P_1 , P_2 , Q_1 , and Q_2 must be chosen such that they verify that

$$y_{F_1}y_{Q_1} - y_{F_2}y_{Q_2} + z_{F_1}z_{Q_1} - z_{F_2}z_{Q_2} \neq 0. \quad (37)$$

Using the calculated value $\widehat{\mathcal{A}c_{G^*}}$ from Eq. (36) and noticing that ω , ρ , e , A , and m are known, we can determine M by solving the nonlinear equation

$$\widehat{\mathcal{A}c_{G^*}} = \frac{-\omega^2}{A\omega\sqrt{M\rho}\cot(k_p e) - m\omega^2}. \quad (38)$$

Recalling that $k_p e = \omega\sqrt{\rho/Me} \ll 1$, we use that $\cot(k_p e) \approx 1/k_p e$. Thus, Eq. (38) can be written as

$$\widehat{\mathcal{A}c_{G^*}} = \frac{-\omega^2}{AM/e - m\omega^2}. \quad (39)$$

Therefore, solving Eq. (39) for M , we find the approximate value

$$M = \frac{e\omega^2(m\widehat{\mathcal{A}c_{G^*}} - 1)}{A\widehat{\mathcal{A}c_{G^*}}}. \quad (40)$$

We can use Eq. (40) as the initial seed value for an iterative algorithm to find the exact value of M that satisfies the nonlinear Eq. (38).

Now, we substitute the calculated value of $\widehat{f_\theta}$ from Eq. (36) and the calculated value of M from Eq. (38) into Eq. (28). Recalling that [26]

$$G = \frac{M(1 - 2\nu)}{2(1 - \nu)} \quad (41)$$

and

$$k_s = \omega\sqrt{\rho/G} = \omega\sqrt{\frac{2\rho(1 - \nu)}{M(1 - 2\nu)}}, \quad (42)$$

we can substitute Eqs. (41) and (42) into Eq. (28). Consequently, the value of ν that satisfies the nonlinear Eq. (28) is found using an iterative algorithm. The initial seed value of ν for the iterative process can be approximately 0.3.

The remaining elastic parameters are finally calculated from M and ν using Eq. (41) and the equations [26]

$$\lambda = \frac{M\nu}{1-\nu}, \quad (43)$$

$$\kappa = \frac{M(1+\nu)}{3(1-\nu)}, \quad (44)$$

and

$$E = \frac{M(1+\nu)(1-2\nu)}{1-\nu}. \quad (45)$$

4.1. Numerical Examples

Numerical experiments were performed to test the methodology described above. A solid plate made of light concrete ($m = 8$ kg, $A = 0.04$ m², $h = 0.333$ m) on top of a viscoelastic layer was considered. The viscoelasticity of the layer was implemented through the Prony series representation of the P-wave modulus function [27, 28]

$$M(t) = M_\infty + M_0 \sum_{i=1}^n \alpha_i e^{-t/\tau_i}, \quad (46)$$

where

$$M_\infty = M_0 \left(1 - \sum_{i=1}^n \alpha_i \right), \quad (47)$$

and n is the total number of Prony series terms. The following values have been considered in the numerical experiments: $n = 2$, $M_0 = 143951$ N/m², $\alpha_1 = 0.5$, $\alpha_2 = 0.25$, $\tau_1 = 0.0005$ s, and $\tau_2 = 0.001$ s.

The geometry of the elastic layer is customarily represented by the shape factor S , which is defined as the ratio of the plane area A to the perimeter area not bonded to the rigid plates [12]. Therefore, in our case $S = \sqrt{A}/4e$. The values of ρ , ν , e , and S for each numerical experiment are given in Table 1.

Table 1: Values of the density ρ , Poisson's ratio ν , thickness e , and shape factor S of the viscoelastic layer used for each numerical experiment.

Experiment	Density (kg/m ³)	Poisson's ratio	Thickness (mm)	Shape factor
1	100	0.45	3.0	16.67
2	200	0.44	3.0	16.67
3	200	0.45	3.0	16.67
4	200	0.46	3.0	16.67
5	200	0.47	3.0	16.67
6	400	0.45	3.0	16.67
7	600	0.45	3.0	16.67
8	200	0.45	2.5	20.00
9	200	0.45	3.5	14.29
10	200	0.45	4.0	12.50

The analysis was performed using ANSYS©. A harmonic force of amplitude 1 N was applied at points $P_1(0.336, 0, 0.1)$ and $P_2(0.336, 0, 0.1)$, and the corresponding acceleration responses were determined at points $Q_1(0.336, 0, 0)$ and $Q_2(0.336, 0, 0.08)$, respectively. The values of M and ν were determined as a function of $\omega = 2\pi f$ using the equations derived in section 4 for frequencies between 0 and 500 Hz. For numerical implementation, the values of M were found by solving the nonlinear equations using Newton's method, and the values of ν were determined from the secant method. The rest of the elastic moduli of the layer (bulk modulus, Young's modulus, shear modulus, and Lamé's first parameter) were obtained using the estimated values for M and ν . The errors in the estimated values were calculated as $\epsilon = 100 \times |V_e - V_a|/V_a$, where V_e is the es-

estimated value and V_a is the actual value. The errors in estimating M and ν were plotted as a function of frequency in Figs. 11, 12, and 13.

It can be seen from Fig. 11 that larger values of density of the layer increase the error in estimating the real part of M at higher frequencies because of the effect of higher modes. However, the error is less than 4% for frequencies below 200 Hz.

From Figs. 11–13 we observe that the absolute percentage error in estimating the Poisson's ratio using the procedure proposed here is between 0.5% and 1.4% for frequencies above 8 Hz. As expected, errors are much larger at lower frequencies as discussed after Eq. (34).

In addition, in Fig. 13 it can be observed that better results are obtained for thinner layers, that is, when the shape factor is increased. Since we are considering a standardized dynamic stiffness test, in which the area is fixed at 0.04 m^2 , the only option for reducing the error would be to reduce the thickness of the layer as much as possible.

It is also noticed that the error in estimating the P-wave modulus, M , increases when Poisson's ratio is near 0.5 (see Fig. 12). This is because the term $1 - 2\nu$ becomes very small as indicated in Eq. (41). The same occurs for E (see Eq. (45)). In the case of $\nu = 0.49$, the errors are approximately 11.2% for M and E between 100 Hz and 500 Hz. However, the errors for the loss factor $\tan \delta$ (the ratio between the imaginary and the real parts of the complex moduli) were consistently smaller than 2% as shown in Fig. 14.

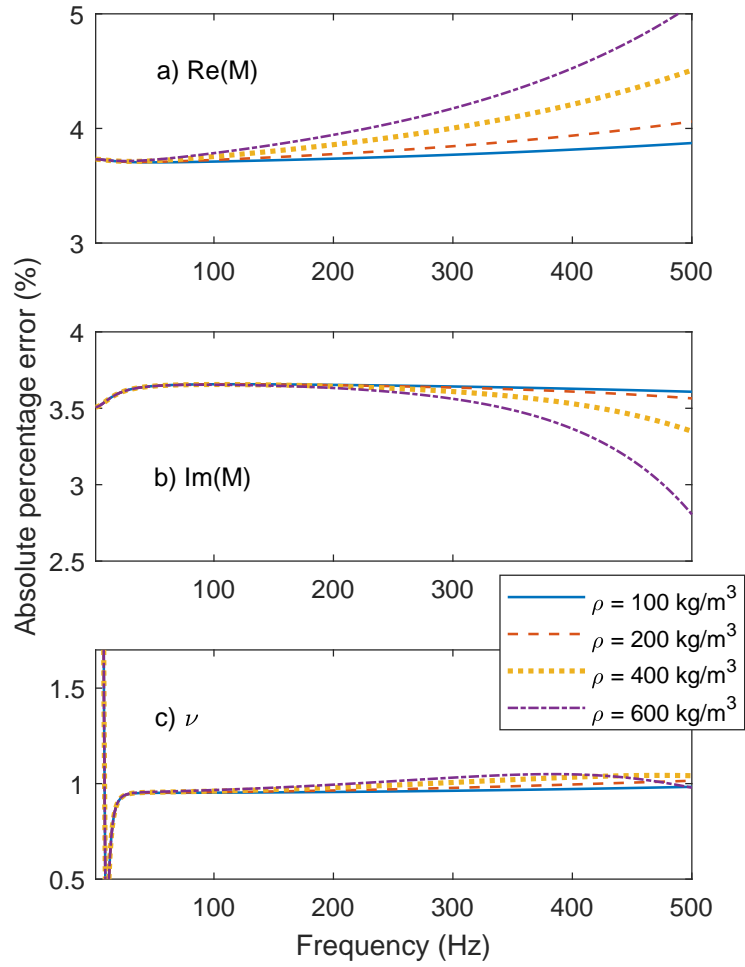


Figure 11: Absolute percentage error in estimating the P-wave modulus M and the Poisson's ratio ν for a viscoelastic layer ($\nu = 0.45$, $e = 3$ mm) with different densities: a) real part of M ; b) imaginary part of M ; c) Poisson's ratio.

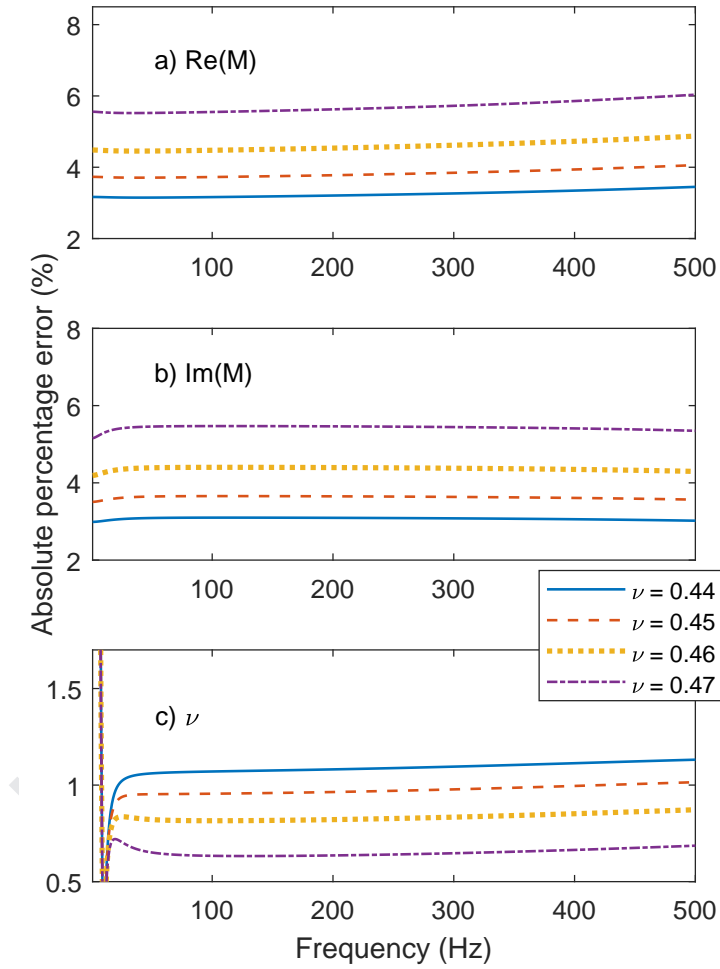


Figure 12: Absolute percentage error in estimating the P-wave modulus M and the Poisson's ratio ν for a viscoelastic layer ($\rho = 200 \text{ kg/m}^3$, $e = 3 \text{ mm}$) with different values of ν : a) real part of M ; b) imaginary part of M ; c) Poisson's ratio.

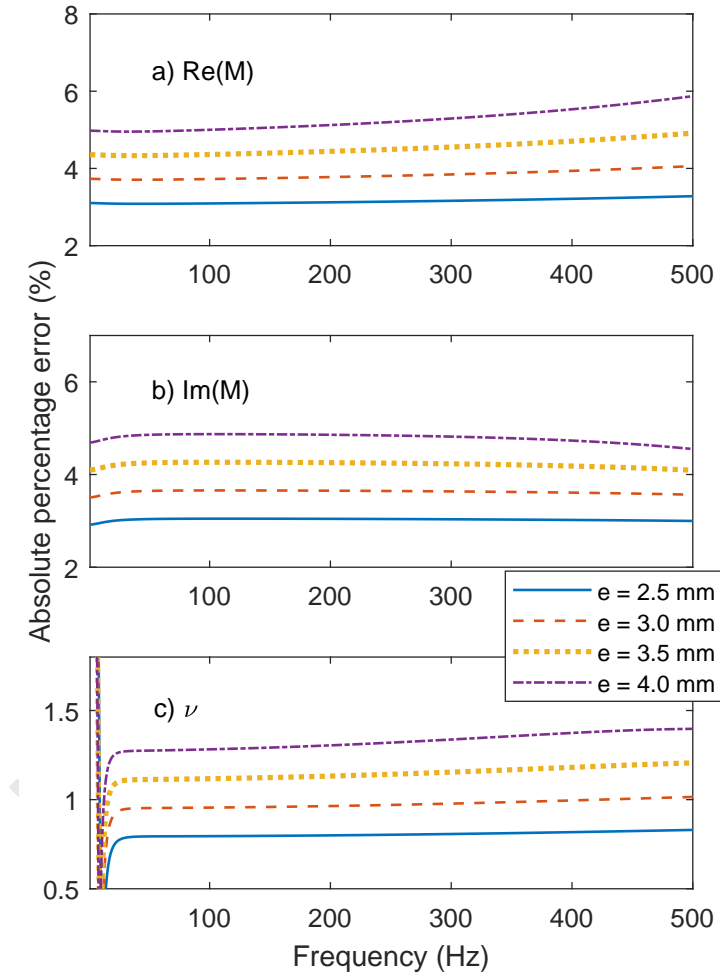


Figure 13: Absolute percentage error in estimating the P-wave modulus M and the Poisson's ratio ν for a viscoelastic layer ($\nu = 0.45$, $\rho = 200 \text{ kg/m}^3$) with different thicknesses: a) real part of M ; b) imaginary part of M ; c) Poisson's ratio.

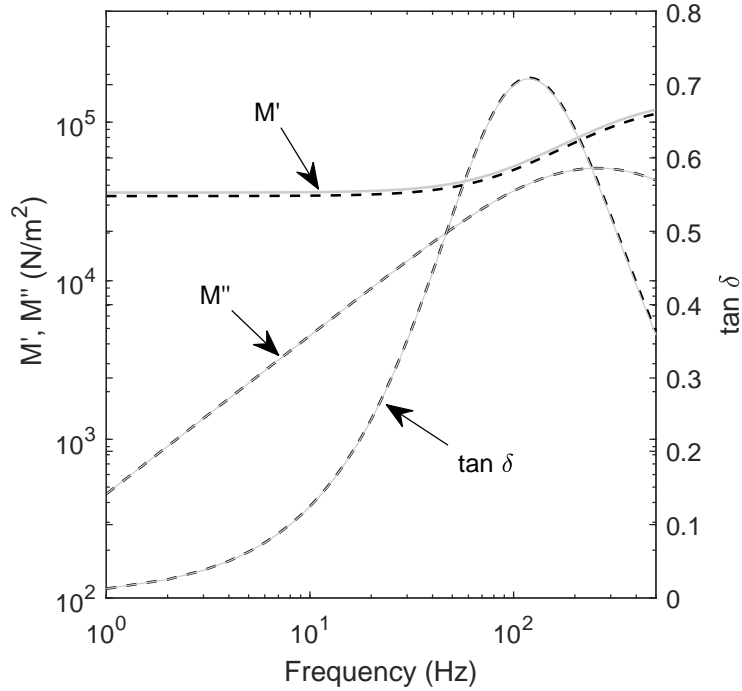


Figure 14: Complex P-wave modulus $M = M' + iM''$ and $\tan \delta = M''/M'$ as a function of frequency for a viscoelastic layer ($\rho = 200 \text{ kg/m}^3$, $\nu = 0.45$, $e = 4 \text{ mm}$). Gray continuous lines: actual values; black dashed lines: estimated values.

5. Conclusions

It should be noted that until now, the analytical solutions for the type of problem posed in this article were based mostly on approaches that required rigorous fulfillment of the equilibrium equations at the boundary. These kinds of solutions depend on the shape of the boundary and present some mathematical complexity. In the present work, a new analytical approach based strictly on the fulfillment of the equations of internal equilibrium has been presented. This approach leads to much simpler analytical expressions that are almost independent of the shape

of the boundary, which makes them easy to implement into computer codes. The expressions depend only on static values such as the area and moments of inertia of the contour.

The new approach presented in this paper provides a useful analytical description of the standardized test commonly used to determine the dynamic stiffness of a material. It has also been shown that the developed analytical solutions may be used to experimentally estimate the elastic parameters of a flexible material, using a harmonic (frequency-dependent) analysis. The only condition is that the plate's chosen material must be much more rigid than the flexible material being tested. It is concluded that the method gives better results when the shape factor is increased, that is, by reducing the thickness of the layer as much as possible.

Acknowledgments

This work was supported by CONICYT-FONDECYT [grant number 1171110].

- [1] E. Freyssinet. Dispositif de liaison elastique a un ou plusieurs degres de liberte (translated as Elastic Device of Connection to One or More Degrees of Freedom). French patent no. 1.110.285 Class F06 d 25/5/54. Ministry of Industry and Commerce, France, 1954.
- [2] Z.-D. Xu, S.-A. Wang, C. Xu, Experimental and numerical study on long-span reticulate structure with multidimensional high-damping earthquake isolation devices, *J. Sound Vib.* 333 (2014) 3044–3057. <https://doi.org/10.1016/j.jsv.2014.02.013>.
- [3] K.N. Kalfas, S.A. Mitoulis, K. Katakalos, Numerical study on the response of steel-laminated elastomeric bearings subjected to variable axial loads

- and development of local tensile stresses, *Eng. Struct.* 134 (2017) 346–357.
<https://doi.org/10.1016/j.engstruct.2016.12.015>.
- [4] M. Östberg, L. Kari, Transverse, tilting and cross-coupling stiffness of cylindrical rubber isolators in the audible frequency range – The wave-guide solution, *J. Sound Vib.* 330 (2011) 3222–3244.
<https://doi.org/10.1016/j.jsv.2011.01.020>.
- [5] J.M. Kelly, *Earthquake-Resistant Design with Rubber*, second ed., Springer, London, 1997. <https://doi.org/10.1007/978-1-4471-0971-6>.
- [6] A.N. Gent, P.B. Lindley, The compression of bonded rubber block, *Proc. Inst. Mech. Eng.* 173 (1959) 111–122.
https://doi.org/10.1243/pime_proc_1959_173_022_02.
- [7] A.N. Gent, E.A. Meinecke, Compression, bending and shear of bonded rubber blocks, *Polymer Eng. Sci.* 10 (1970) 48–53.
<https://doi.org/10.1002/pen.760100110>.
- [8] M.S. Chalhoub, J.M. Kelly, Reduction of the Stiffness of Rubber Bearings due to Compressibility, Report No. UCB/SEMM-86/06, Department of Civil Engineering, University of California, Berkeley, 1987.
- [9] M.S. Chalhoub, J.M. Kelly, Effect of bulk compressibility on the stiffness of cylindrical base isolation bearings, *Int. J. Solids Struct.* 26 (1990) 743–760.
[https://doi.org/10.1016/0020-7683\(90\)90004-f](https://doi.org/10.1016/0020-7683(90)90004-f).
- [10] M.S. Chalhoub, J.M. Kelly, Analysis of infinite-strip-shaped base isolator with elastomer bulk compression, *J. Eng. Mech. (ASCE)* 117 (1991) 1791–1805. [https://doi.org/10.1061/\(asce\)0733-9399\(1991\)117:8\(1791\)](https://doi.org/10.1061/(asce)0733-9399(1991)117:8(1791)).

- [11] M.H.B.M. Shariff, A general approach to axial deformation of bonded elastic mounts of various cross-sectional shapes, *Appl. Math. Model.* 17 (1993) 430–436. [https://doi.org/10.1016/0307-904x\(93\)90118-z](https://doi.org/10.1016/0307-904x(93)90118-z).
- [12] H.-C. Tsai, W.-J. Pai, Simplified stiffness formulae for elastic layers bonded between rigid plates, *Eng. Struct.* 25 (2003) 1443–1454. [https://doi.org/10.1016/s0141-0296\(03\)00044-0](https://doi.org/10.1016/s0141-0296(03)00044-0).
- [13] D. Konstantinidis, S.R. Moghadam, Compression of unbonded rubber layers taking into account bulk compressibility and contact slip at the supports, *Int. J. Solids Struct.* 87 (2016) 206–221. <https://doi.org/10.1016/j.ijsolstr.2016.02.008>
- [14] G. Barone, M. Di Paola, F. Lo Iacono, G. Navarra, Viscoelastic bearings with fractional constitutive law for fractional tuned mass dampers, *J. Sound Vib.* 344 (2015) 18–27. <https://doi.org/10.1016/j.jsv.2015.01.017>.
- [15] L. Wang, S. Li, S. Yao, D. Lv, P. Jia, Study on the vertical stiffness of the spherical elastic layer bonded between rigid surfaces, *Arch. Appl. Mech.* 87 (2017) 1243–1253. <https://doi.org/10.1007/s00419-017-1246-9>.
- [16] F. Zhou, Z. Zhang, D. Wua, H. Zhu, An analytical model for predicting the lateral-torsion coupling property of laminated rubber bearings, *J. Sound Vib.* 427 (2018) 1–14. <https://doi.org/10.1016/j.jsv.2018.04.018>.
- [17] S. Qiao, N. Lu, Analytical solutions for bonded elastically compressible layers, *Int. J. Solids Struct.* 58 (2015) 353–365. <https://doi.org/10.1016/j.ijsolstr.2014.11.018>.

- [18] L. Kari, On the wave-guide modelling of dynamic stiffness of cylindrical vibration isolators. Part I: the model solution, and experimental comparison, *J. Sound Vib.* 244 (2001) 211–233. <https://doi.org/10.1006/jsvi.2000.3468>.
- [19] L. Kari, On the wave-guide modelling of dynamic stiffness of cylindrical vibration isolators. Part II: the dispersion relation solution, convergence analysis and comparison with simple models, *J. Sound Vib.* 244 (2001) 235–257. <https://doi.org/10.1006/jsvi.2000.3469>.
- [20] D.D. Ebenezer, K. Ravichandran, C. Padmanabhan, Forced vibrations of solid elastic cylinders, *J. Sound Vib.* 282 (2005) 991–1007. <https://doi.org/10.1016/j.jsv.2004.03.070>.
- [21] S. Qiao, N. Lu, Stress analysis for nanomembranes under stamp compression, *Extreme Mech. Lett.* 7 (2016) 136–144. <https://doi.org/10.1016/j.eml.2016.02.002>.
- [22] J.-Y. Lee, J.-M. Kim, J. Kim, J. Kim, Evaluation of the long-term sound reduction performance of resilient materials in floating floor systems, *J. Sound Vib.* 366 (2016) 199–210. <https://doi.org/10.1016/j.jsv.2015.11.046>.
- [23] ISO 9052-1. Acoustics – Determination of dynamic stiffness – Part 1: Materials used under floating floors in dwellings, International Organization for Standardization, Geneva, 1989.
- [24] C. Hopkins, *Sound Insulation*, Elsevier, Oxford, 2007. <https://doi.org/10.4324/9780080550473>.
- [25] F.P. Beer, E.R. Johnston, P. Cornwell, B. Self, *Vector Mechanics for Engineers: Dynamics*, eleventh ed., McGraw-Hill, New York, 2015.

- [26] W.S. Slaughter, *The Linearized Theory of Elasticity*, Birkhauser, Boston, 2002. <https://doi.org/10.1007/978-1-4612-0093-2>.
- [27] H. Ucar, I. Basdogan, Vibration response prediction on rubber mounts with a hybrid approach, *Int. J. Acoust. Vib.* 23 (2018) 57–64. <https://doi.org/10.20855/ijav.2018.23.11109>.
- [28] R.M. Christensen, *Theory of Viscoelasticity: An Introduction*, second ed., Academic Press, New York, 1986. <https://doi.org/10.1016/B978-0-12-174252-2.X5001-7>.

- A new analytical approach linked with multilayer elastomeric bearings is proposed
- Derived equations provide a useful analytical description of a standardized test
- The new approach leads to solutions that are easy to implement into computer codes
- The approach can be used to estimate the elastic parameters of a flexible material

Journal Pre-proof